

Compound-specific carbon isotopes from Earth's largest flood basalt eruptions directly linked to the end-Triassic mass extinction

Jessica H. Whiteside^{a,1}, Paul E. Olsen^{b,1}, Timothy Eglinton^c, Michael E. Brookfield^d, and Raymond N. Sambrotto^e

^aDepartment of Geological Sciences, Brown University, Box 1846, Providence, RI 02912; ^bDepartment of Earth and Environmental Sciences, Lamont-Doherty Earth Observatory of Columbia University, Palisades, NY 10964; ^cDepartment of Marine Geology and Geophysics, Woods Hole Oceanographic Institution, Woods Hole, MA 02543; ^dInstitute of Earth Sciences Academia Sinica, Nankang, Taipei 11529, Taiwan; and ^eLamont-Doherty Earth Observatory of Columbia University, Palisades, NY 10964

Contributed by Paul E. Olsen, February 12, 2010 (sent for review January 12, 2010)

A leading hypothesis explaining Phanerozoic mass extinctions and associated carbon isotopic anomalies is the emission of greenhouse, other gases, and aerosols caused by eruptions of continental flood basalt provinces. However, the necessary serial relationship between these eruptions, isotopic excursions, and extinctions has never been tested in geological sections preserving all three records. The end-Triassic extinction (ETE) at 201.4 Ma is among the largest of these extinctions and is tied to a large negative carbon isotope excursion, reflecting perturbations of the carbon cycle including a transient increase in CO₂. The cause of the ETE has been inferred to be the eruption of the giant Central Atlantic magmatic province (CAMP). Here, we show that carbon isotopes of leaf wax derived lipids (*n*-alkanes), wood, and total organic carbon from two orbitally paced lacustrine sections interbedded with the CAMP in eastern North America show similar excursions to those seen in the mostly marine St. Audrie's Bay section in England. Based on these results, the ETE began synchronously in marine and terrestrial environments slightly before the oldest basalts in eastern North America but simultaneous with the eruption of the oldest flows in Morocco, a CO₂ super greenhouse, and marine biocalcification crisis. Because the temporal relationship between CAMP eruptions, mass extinction, and the carbon isotopic excursions are shown in the same place, this is the strongest case for a volcanic cause of a mass extinction to date.

astrochronology | CO₂ | Jurassic | large igneous provinces | *n*-alkane

Plants record through photosynthetic pathways the atmospheric values of $\delta^{13}\text{C}$ that in turn reflect the exchangeable surface oceanic carbon reservoir (1). One of the most direct known plant proxies is the $\delta^{13}\text{C}_{\text{alk}}$ measurements of *n*-C₂₅–*n*-C₃₁ *n*-alkanes derived from leaf wax lipids of plant cuticles (2). We analyzed $\delta^{13}\text{C}_{\text{alk}}$, the carbon isotopic composition of wood ($\delta^{13}\text{C}_{\text{wood}}$), and total organic carbon ($\delta^{13}\text{C}_{\text{toc}}$) from sediments from two overlapping lacustrine sections interbedded with the lavas of the Central Atlantic magmatic province (CAMP) (3) in eastern North America to obtain a carbon isotope record unambiguously tied to the eruptions and climate proxies to compare with and calibrate organic carbon and carbonate $\delta^{13}\text{C}$ records from elsewhere (3–7). This allows direct determination of the relationship between one of the largest Phanerozoic mass extinctions, the end-Triassic extinction (ETE) (8), carbon isotopic and CO₂ (9) excursions, the biocalcification crisis (10), and their proposed cause, the CAMP (3, 11–13). Core and outcrop samples were obtained from the Newark (New York, New Jersey, and Pennsylvania) and Hartford (Connecticut and Massachusetts) rift basins at 19–20° N paleolatitude (14) in the tropical humid to arid transition of central Pangea (Fig. 1). A hierarchy of Milankovitch-forced lake level cycles permeate the sampled strata in these basins, and in conjunction with a high sediment accumulation rate and magnetostratigraphic and radioisotopic calibration (*SI Text* and *Datasets S1–S3*), a 2.4 m.y. unbroken record of events

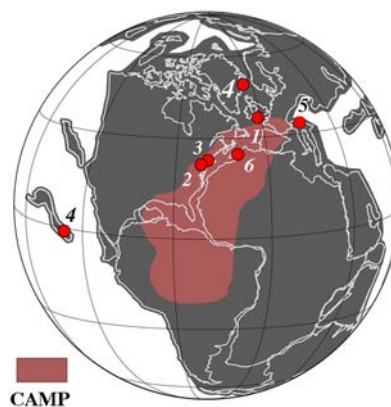


Fig. 1. Map of Pangea at 201 Ma showing the distribution of the CAMP and the localities discussed in the text: 1, St. Audrie's Bay; 2, Newark basin; 3, Hartford basin; 4, Kennecott Point; 5, Val Adrara; 6, Moroccan CAMP sections. Base map (orthographic projection) courtesy of C. Scotese based on the latitudinal positions of ref. 14.

surrounding the ETE can be placed into the high-precision (<20 ky) Newark/Hartford basin astronomically calibrated geomagnetic polarity time scale (NBAGPTS) (15–17) (Fig. 2). The combined section is registered to the marine record by high-resolution magnetostratigraphy (17, 18), high-precision U–Pb ages, and cyclostratigraphy (7, 19), and spans the late Rhaetian of the Late Triassic to the early Sinemurian of the Early Jurassic (Fig. 2). Our data indicate the *n*-alkanes from these strata preserve an original leaf wax signal (*SI Text*).

Carbon Isotope Results

All three sets of carbon isotopic data from the Newark and Hartford basin sections show considerable variability seemingly tied in part to the lacustrine cyclicity (spanning approximately 9‰ in $\delta^{13}\text{C}_{\text{alk}}$, approximately 7‰ in $\delta^{13}\text{C}_{\text{wood}}$, and approximately 15‰ in $\delta^{13}\text{C}_{\text{toc}}$) through the section, but show largely parallel trends around the ETE (Fig. 2). Specifically, there is an approximately 2–4‰ shift to ¹³C-depleted values exactly at the ETE and associated fern spike (16) as reflected in the Newark and Hartford basins. The duration of this distinct excursion in the Newark and Hartford basins is only about 20–40 ky. This is succeeded by a distinct ¹³C-enriched interval (by approximately

Author contributions: J.H.W. and P.E.O. designed research; J.H.W., P.E.O., and M.E.B. performed research; J.H.W., P.E.O., T.E., and R.N.S. analyzed data; and J.H.W. and P.E.O. wrote the paper.

The authors declare no conflict of interest.

¹To whom correspondence may be addressed. E-mail: Jessica_Whiteside@Brown.edu or polsen@ldeo.columbia.edu.

This article contains supporting information online at www.pnas.org/cgi/content/full/1001706107/DCSupplemental.

a change in contribution of different organisms, a possibility suggested for the origin of the initial excursion at other localities (6). Thus, a change in community structure is likely responsible for at least part of the initial excursion as seen at the St. Audrie's Bay section. This interval shows an unusual abundance of fern spores but no exceptional concentration of organic-walled aquatic organisms at St. Audrie's Bay (20), suggesting a terrestrial ecosystem change. The duration of the initial excursion at St. Audrie's Bay has been independently estimated at 20–40 ky (7) in agreement with our estimates based on the Newark–Hartford data.

The initial excursion thus can be identified as beginning at the extinction level in the Newark basin possibly extending through the time of the deposition of the oldest CAMP lava flows. Critically, extinctions persist into strata postdating the initial excursion (e.g., conodonts) at St. Audrie's Bay (20) and elsewhere, demonstrating that extinctions persisted a short time after the initial CAMP pulse.

Discussion

Both the combined Newark and Hartford $\delta^{13}\text{C}_{\text{alk}}$ and the St. Audrie's Bay $\delta^{13}\text{C}_{\text{alk}}$ data exhibit oscillations in values younger and older than the initial excursion that are not directly connected with extinctions, but rather track the lacustrine cyclicity and exhibit coherent power around an approximately 100 ky periodicity (Fig. 3) (SI Text). $\delta^{13}\text{C}_{\text{alk}}$ and $\delta^{13}\text{C}_{\text{toc}}$ are also coherent around approximately 100 ky. The magnitude of these oscillations decreases after the positive excursion following the initial excursion, and we suggest they reflect climate-related ecological changes altering both the taxonomic composition of the plant communities supplying the waxes and the isotopic discrimination of the members of the community under highly stressed conditions. With only the two available fiducials (the ETE and the Sinemurian–Hettangian boundary), the St. Audrie's $\delta^{13}\text{C}_{\text{alk}}$ and $\delta^{13}\text{C}_{\text{toc}}$ data also exhibit coherent approximately 100 ky periodicity using the NBAGPTS for temporal constraints. The thickness periodicities are also fully consistent with those seen in $\delta^{13}\text{C}_{\text{toc}}$, percent total organic carbon, and percent carbonate described in ref. 7 (Fig. 3), again very strongly suggesting that both the time scale and the correlation between the two sections are correct.

Although the isotopic excursion and ETE predate the onset of CAMP in the Newark and Hartford basins, the lava flows in these basins do not reflect the full temporal extent of the eruptions. The Culpeper basin of Virginia and Argana and Central High Atlas basins of Morocco demonstrate that the CAMP eruptions were more extensive than the three flow sequences preserved in the Newark and Hartford basins (23) (Fig. 4). In addition, some CAMP flows in Morocco are most likely slightly older than those recognized in eastern North America (24, 25) (SI Text). These older flows may be synchronous with the initiation of the ETE.

It is unlikely that the initial excursion seen at St. Audrie's Bay and in eastern North America was generated by mantle CO_2 alone, because of the similarity in atmospheric and mantle $\delta^{13}\text{C}$ values (26). Hence, an injection of ^{12}C carbon from CAMP-triggered methane clathrates (4, 9) dissociation or thermogenic methane (27) release from intrusive metamorphism (13) has been hypothesized. One alternative is that an intensification of the hydrological cycle, as a result of greater CO_2 -forced warming causing an increase in available moisture driving greater isotopic discrimination (28) caused a shift toward more ^{13}C -depleted values in the plant wax *n*-alkanes. This is entirely consistent with the enhanced lacustrine cyclicity and *n*-alkane cyclicity in the Newark and Hartford data after the ETE. A concurrent shutoff of the biological pump would result in a homogenization of the water column caused by the extinction of zooplankton grazers (cf. K-T boundary in ref. 29) with surface waters becoming enriched in ^{12}C . The short duration of the initial excursion is also incompatible with the modeled estimates of the

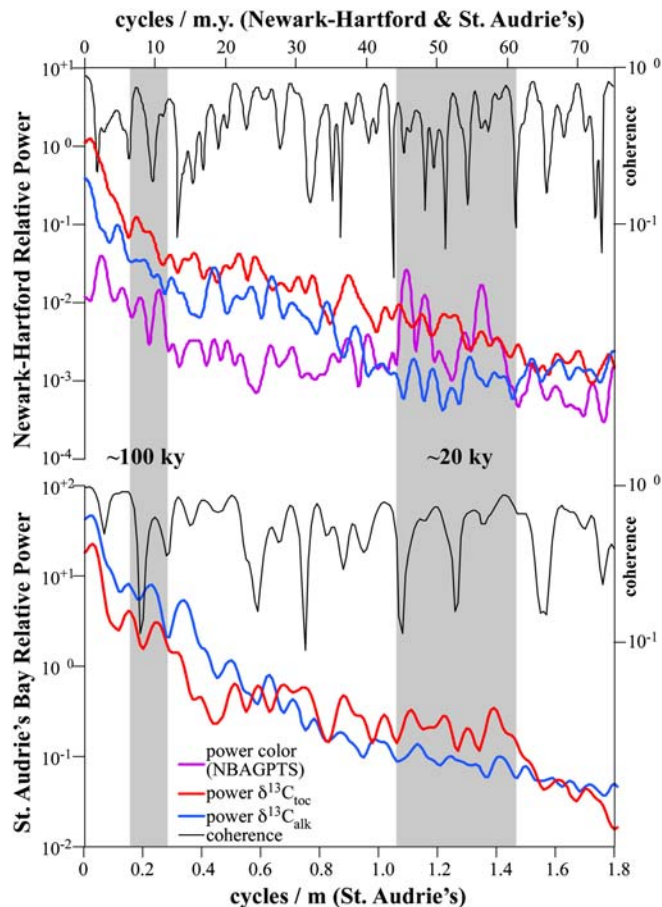


Fig. 3. Comparison between power spectra of carbon isotopic data from the Newark and Hartford basins and the St. Audrie's Bay section using the same time scale (NBAGPTS) based on the correlation to the base of the ETE and the Hettangian–Sinemurian boundary. Note the correspondence between the approximately 100 ky periods in $\delta^{13}\text{C}_{\text{alk}}$ and $\delta^{13}\text{C}_{\text{toc}}$ in both the Newark–Hartford and St. Audrie's data and the presence of the approximately 20 ky cycle in the St. Audrie's $\delta^{13}\text{C}_{\text{toc}}$ data. Coherence in the Newark–Hartford data and in the St. Audrie's data is shown between the $\delta^{13}\text{C}_{\text{alk}}$ and $\delta^{13}\text{C}_{\text{toc}}$ with the spectrum for color shown for reference as it is tuned to the NBAGPTS. Nonzero coherence is greater than 0.6.

recovery time from a methane clathrates dissociation event by over an order of magnitude (20–40 ky compared to 700–1000 ky from ref. 26). Other proposed killing mechanisms include CAMP-outgassed or metamorphism-related volatiles such as sulfuric acid (27) or halogens (13, 30); however, none of these models have yielded unique predictions testable in the sedimentary record. We also cannot exclude a role for a bolide impact as a killing mechanism, although evidence consisting mostly of modest Ir anomalies (16) is also compatible with a volcanic origin.

Carbonate $\delta^{13}\text{C}$ records from St. Audrie's Bay (31) track the $\delta^{13}\text{C}_{\text{toc}}$ and $\delta^{13}\text{C}_{\text{alk}}$ data, which in turn match the variations in the Newark and Hartford $\delta^{13}\text{C}_{\text{alk}}$ data that are orbitally paced. Because the St. Audrie's Bay carbonate data are unlikely to have been affected by local community change without some process linking them via the exchangeable carbon reservoirs, there seems to have been a significant role for orbital cycles pacing the Earth's exchangeable reservoirs as has been suggested for a number of other isotopic excursions (32). However, the behavior of *n*-alkanes in the initial excursion is qualitatively different from the other fluctuations, suggesting a different origin such as the effects of the initial influx of greenhouse gases and the extinctions themselves, the exact expression of which would be influenced by synergetic changes in the local conditions and local communities

The negative $\delta^{13}\text{C}$ excursions in the Newark, Hartford, and St. Audrie's Bay documented by the *n*-alkane, wood, total organic carbon data, and the correlations to Jamesonland strongly suggest a massive input of ^{13}C -depleted CO_2 and/or other greenhouse gases coincident with the onset of CAMP. The very tight association between the onset of the CAMP and the abrupt extinctions in the tropics and subtropics, the more protracted extinctions well into the CAMP episode in the higher latitudes during the time of maximum eruptive rate, and the association of the elevated CO_2 levels tied to the entire known CAMP episode strongly argues for a major causative role for CAMP-generated CO_2 in the extinctions themselves. Our interpretation of the carbon isotopic data from these continental and marine sections provides strong direct evidence by direct superposition that the eruption of a giant flood basalt province could cause a climatic catastrophe resulting in a major mass extinction.

Methods

For *n*-alkane extraction, approximately 4–12 g of powdered sedimentary rock samples were extracted on a Dionex Accelerated Solvent Extraction system using three washes of dichloromethane (DCM) or 9:1 DCM/methanol to produce a total lipid extract (TLE). The TLE was saponified with 0.5N KOH/methanol, and then extracted with hexane. This neutral extract was dried with anhydrous Na_2SO_4 to remove traces of water, then eluted from a silica gel column (1 mL bed volume, silica gel 2% deactivated) into two fractions, first a hexane elutable and second a combined DCM and methanol elutable fraction. If required, the hexane elutable fraction was further fractionated into adduct [straight chain ($\text{C} \geq 14$) *n*-alkanes] and nonadduct fractions by urea adduction, or by sequestering the straight chain alkanes in zeolites, rinsing with hexane, and alkane recovery by dissolution of the zeolite with aqueous HF.

Compound-specific carbon isotopic measurements were determined by isotope ratio monitoring–gas chromatography/mass spectrometry using a Thermo DeltaVPlus MS coupled to an Agilent 6890 GC via a GCC-III combustion interface at Brown University. The $\delta^{13}\text{C}$ values for individual compounds were determined based on introduction of reference CO_2 gas pulses (previously and subsequently calibrated with a series of well-characterized standard materials), reported as means of duplicate runs ($\sigma = \pm 0.3$ to 0.6), and expressed in ‰ relative to the Pee Dee belemnite (PDB). The bulk organic matter of sediment wood was analyzed to determine the ratio of $^{13}\text{C}/^{12}\text{C}$ by mass spectrometry. The samples were cleaned with deionized water, air-dried, ground into a fine powder with a ceramic mortar and pestle, fumed with 37% HCl in a bell jar at 60 °C for 50 h (to remove recalcitrant carbonate), and dried above a plate of silica gel desiccant at 60 °C for at least 24 h. All samples were weighed into silver capsules, with mass determined by total organic-carbon (TOC) content, grouped according to TOC, and processed with an automated micro-Dumas combustion technique using a Europa ANCA system plumbed into a 20-20-NT continuous flow mass spectrometer system at Lamont-Doherty Earth Observatory. C isotope ratios were measured against National Institute of Standards and Technology and International Atomic Energy Agency standard reference materials and combusted in the same manner as the samples (glucosamine, $\delta^{13}\text{C} = -20.80$, C = 20.50%; methionine, $\delta^{13}\text{C} = 25.10$, C = 40.25% (Cornell only), all versus the PDB ($^{13}\text{C}/^{12}\text{C} = 11237.2 \pm 60 \times 10^{-6}$). Precision of the analytical system is 0.12‰ for C at the typical sample sizes (4 μm C) used here.

Time series analysis was performed using Analyseries 2.037 (37).

ACKNOWLEDGMENTS. We thank Daniel Montluçon, Carl Johnson, and Camly Tran for laboratory assistance. We are grateful to Micha Ruhl for permission to use the St. Audrie's Bay $\delta^{13}\text{C}$ curve from refs. 7 and 19. We also thank Michael Rampino and Randall Irmis for reviewing the manuscript. J.H.W. and P.E.O. acknowledge support from the US National Science Foundation (Grant EAR 0801138 to J.H.W. and Grant EAR 0753496 to P.E.O.).

- Farquhar GD, Ehleringer JR, Hubick KT (1989) Carbon isotope discrimination and photosynthesis. *Annu Rev Plant Physiol Plant Mol Biol* 40:503–537.
- Eglinton G, Hamilton RJ (1967) Leaf epicuticular waxes. *Science* 156:1322–1335.
- Marzoli A, et al. (1999) Extensive 200-million-year-old continental flood basalts of the Central Atlantic Magmatic Province. *Science* 284:616–618.
- Hesselbo SP, et al. (2002) Terrestrial and marine extinction at the Triassic-Jurassic boundary synchronized with major carbon-cycle perturbation: A link to initiation of massive volcanism?. *Geology* 30:251–254.
- Williford KH, et al. (2007) An extended stable organic carbon isotope record across the Triassic-Jurassic boundary in the Queen Charlotte Islands, British Columbia, Canada. *Palaeogeogr Palaeoclimatol* 244:290–296.
- Kürschner WM, Bonis NR, Krystyn L (2007) Carbon-isotope stratigraphy and palynostratigraphy of the Triassic-Jurassic transition in the Tiefengraben section –Northern Calcareous Alps (Austria). *Palaeogeogr Palaeoclimatol* 244:257–280.
- Ruhl M, et al. Astronomical constraints on the duration of the Early Jurassic Hettangian stage and recovery rates following the end-Triassic mass extinction (St. Audrie's Bay/East Quantoxhead, UK). *Earth Planet Sci Lett*, in press.
- Benton MJ (1995) Diversification and extinction in the history of life. *Science* 268:52–58.
- McElwain JC, Wagner PJ, Hesselbo SP (2009) Fossil plant relative abundances indicate sudden loss of Late Triassic biodiversity in East Greenland. *Science* 324:1554–1556.
- van de Schootbrugge B, et al. (2007) End-Triassic calcification crisis and blooms of organic-walled 'disaster species'. *Palaeogeogr Palaeoclimatol* 244:126–141.
- Rampino MR, Stothers RB (1988) Flood basalt volcanism during the past 250 million years. *Science* 241:663–668.
- Wignall PB (2001) Large igneous provinces and mass extinctions. *Earth-Sci Rev* 53:1–33.
- Ganino C, Arndt NT (2009) Climate changes caused by degassing of sediments during the emplacement of large igneous provinces. *Geology* 37:323–326.
- Kent DV, Tauxe L (2005) Corrected Late Triassic latitudes for continents adjacent to the North Atlantic. *Science* 307:240–244.
- Kent DV, Olsen PE (1999) Astronomically tuned geomagnetic polarity time scale for the Late Triassic. *J Geophys Res* 104:12831–12841.
- Olsen PE, et al. (2002) Ascent of dinosaurs linked to an iridium anomaly at the Triassic-Jurassic boundary. *Science* 296:1305–1307.
- Kent DV, Olsen PE (2008) Early Jurassic magnetostratigraphy and paleolatitudes from the Hartford continental rift basin (eastern North America): Testing for polarity bias and abrupt polar wander in association with the central Atlantic magmatic province. *J Geophys Res* 113:B06105 doi: 10.1029/2007JB005407.
- Muttoni G, et al. (2004) Tethyan magnetostratigraphy from Pizzo Mondello (Sicily) and correlation to the Late Triassic Newark astrochronological polarity time scale. *Geol Soc Am Bull* 116:1043–1058.
- Ruhl M (2010) Carbon cycle changes during the Triassic–Jurassic transition. *Laboratory of Paleobotany and Palynology, Contribution Series 28* (Utrecht Univ, The Netherlands).
- Hounslow MW, Posen PE, Warrington G (2004) Magnetostratigraphy and biostratigraphy of the Upper Triassic and lowermost Jurassic succession, St. Audrie's Bay, UK. *Palaeogeogr Palaeoclimatol* 213:331–358.
- Schoene B, et al. A correlation between the Triassic-Jurassic boundary mass extinction and flood basalt eruption at the 100 ka-level using ID-TIMS U/Pb zircon geochronology. *Geology*, in press.
- Schaltegger U, et al. (2008) Precise U-Pb age constraints for end-Triassic mass extinction, its correlation to volcanism and Hettangian postextinction recovery. *Earth Planet Sci Lett* 267:266–275.
- Whiteside JH, et al. (2007) Synchrony between the CAMP and the Triassic-Jurassic mass-extinction event?. *Palaeogeogr Palaeoclimatol* 244:345–367.
- Marzoli A, et al. (2004) Synchrony of the Central Atlantic magmatic province and the Triassic-Jurassic boundary climatic and biotic crisis. *Geology* 32:973–976.
- Deenen MHL, et al. (2010) A new chronology for the end-Triassic mass extinction. *Earth Planet Sci Lett* 291:113–125.
- Beerling DJ, Berner RA (2002) Biogeochemical constraints on the Triassic-Jurassic boundary carbon cycle event. *Global Biogeochem Cycles* 16:10-1–10-16 doi: 10.1029/2001GB001637.
- van de Schootbrugge B, et al. (2009) Floral changes across the Triassic/Jurassic boundary linked to flood basalt volcanism. *Nat Geosci* 2:589–594.
- Bowen GJ, et al. (2004) A humid climate state during the Palaeocene/Eocene thermal maximum. *Nature* 432:495–499.
- D'Hondt SD (2005) Consequences of the Cretaceous/Paleogene mass extinction for marine ecosystems. *Annu Rev Ecol Syst* 36:295–317.
- Svensen H, et al. (2009) Siberian gas venting and the end-Permian environmental crisis. *Earth Planet Sci Lett* 277:490–500.
- Korte C, et al. (2009) Paleoenvironmental significance of carbon-and oxygen-isotope stratigraphy of marine Triassic-Jurassic boundary sections in SW Britain. *J Geol Soc London* 166:431–445.
- Kemp DB, et al. (2005) Astronomical pacing of methane release in the Early Jurassic Period. *Nature* 437:396–399.
- Cohen AS, Coe AL (2002) New geochemical evidence for the onset of volcanism in the Central Atlantic Magmatic Province and environmental change at the Triassic-Jurassic boundary. *Geology* 30:267–270.
- Cornet B (1977) The palynostratigraphy and age of the Newark Supergroup. PhD thesis (Pennsylvania State Univ, University Park, PA).
- Bonis NR, et al. (2009) Climate change driven black shale deposition during the end-Triassic in the western Tethys. *Palaeogeogr Palaeoclimatol* doi: 10.1016/j.palaeo.2009.06.016.
- Smith FA, et al. (2007) Magnitude of the carbon isotope excursion at the Paleocene-Eocene thermal maximum: The role of plant community change. *Earth Planet Sci Lett* 262:50–65.
- Paillard D, Labeyrie L, Yiou P (1996) Macintosh program performs time-series analysis. *Eos Trans AGU* 77:379.
- Morton N (2008) Details of voting on proposed GSSP and ASSP for the base of the Hettangian Stage and Jurassic System. *Int Subcomm Jurassic Stratigr Newslett*, 35 p:74.
- Ruhl M, Kürschner WM, Krystyn L (2009) Triassic–Jurassic organic carbon isotope stratigraphy of key sections in the western Tethys realm (Austria). *Earth Planet Sci Lett* 281:169–187.

Supporting Information

Whiteside et al. 10.1073/pnas.1001706107

SI Text

Evidence that These Molecules Originate Predominately from Indigenous Vascular Plants. The saturate fraction of extractions from multiple samples from the Hartford-Newark and St. Audrie's Bay section (Datasets S1 and S3) show an odd-over-even preference for the C_{25-31} *n*-alkanes, characteristic of an origin from vascular plant cuticular waxes (1). Further evidence of this origin is indicated by their high carbon preference index (CPI) and relatively low thermal alteration, consistent with published data that indicates that much of the Jurassic Newark–Hartford section in the upper part of the oil window and that the St. Audrie's section is thermally immature (Fig. S1 and Dataset S3). Newark and Hartford extractions generally have less obvious carbon preference, and some have CPIs characteristic of hydrocarbons generated from the organic matter (Fig. S1 and Dataset S1). Because of the very high Newark and Hartford basin accumulation rates, the relatively very small volumes of organic rich strata and the observed differences in *n*-alkane FID chromatograms and $\delta^{13}C$ values between samples only a few meters apart (Fig. S1), the Newark and Hartford $\delta^{13}C_{alk}$ values represent local, in situ hydrocarbons from indigenous organic matter. They are thus most simply interpreted as representative of the original *n*-alkane values. This is consistent with published thermal maturity data that indicate low thermal maturity ($R_0 = 0.4 - 1.0$; see refs. 2–4) of Newark and Hartford samples, just within the oil window.

Supporting Paleomagnetic Correlations. Hounslow et al. (5) document the presence of a thin reverse interval above the initial excursion (zone SA5r), with the rest of their postinitial sampled stratigraphy being of normal polarity. It is our contention that this reverse polarity zone should correlate to the section immediately above the Orange Mountain Basalt, but no reverse polarity zones were found in the Newark basin coring project sampling of that interval (lower Feltville Formation). Three lines of evidence lead us to argue they may have been missed by the initial sampling. First, the lower Feltville Formation is largely gray and black beds that were not sampled by Kent et al. (1995) because of their less favorable magnetic behavior compared to red beds, and thus most of the lower Feltville was not sampled. Second, the lower Feltville Formation in the Martinsville no. 1 core is highly condensed compared to elsewhere in the basin (Olsen et al., 1996a) and the reverse zone could easily be omitted. Third, two thin zones of reverse polarity have been identified in interbedded cyclical lacustrine strata and Central Atlantic magmatic province (CAMP) basalts of the Central High Atlas, Morocco (Knight et al., 2004) correlative to the lower Feltville Formation (Whiteside et al., 2007), and three thin zones of reverse polarity occur close to and above the extinction level in the Moncornet core in the Paris basin (6). Such stratigraphically thin polarity zones are easy to miss and difficult to interpret, but their presence in multiple sections leads us to interpret reverse polarity zone SA5r at St. Audrie's as correlative with one of the two, probably the upper, reverse zone in the Central High Atlas and one of the upper two in the Moncornet core. Additional sampling of eastern North American strata is underway to locate these polarity zones within the Newark and Fundy basin sections.

***n*-Alkane Data from Newark and Hartford Basins and St. Audrie's Bay.** For the Newark and Hartford basins (Datasets S1 and S2), the

data are placed in the orbitally calibrated time scale of Whiteside et al. (7) and Kent and Olsen (8). Samples are registered into the detailed litho- and cyclostratigraphy from each basin section, for the most part based on core or long outcrop transects. A synthetic target climatic precession curve, described in ref. 7, was constructed using the values for *k* (precessional constant, from ref. 9) for the Late Triassic–Early Jurassic (approximately 200 Ma) and values of *g*₃ and *g*₄ (fundamental frequencies of Earth and Mars), derived from the empirical observations of the frequency of the beat cycle (*g*₃–*g*₄) of these frequencies visible in the Newark basin record (10). Inasmuch as there are infinite solutions to the *g*₃–*g*₄ equation for a single value (two variables and two unknowns), we use the average within the chaotic zone as defined by Laskar et al. (11), for the empirical value for *g*₃–*g*₄ of 1/1.75 m.y. (10), with amplitudes derived from ref. 12. The sections in the depth domain were then tuned to the target curve using the lineage option of Anlyseries (13) assuming that the peak values in depth ranks correspond to precessional maxima. The St. Audrie's Bay data (Dataset S3) are placed within the depth scale of Ruhl et al. (14, 15).

CPI and Average Chain Length. CPI was calculated using a modified version of the “improved” (CPI2) method (16) using the following formula:

$$\frac{1}{2} \left(\frac{(A_{25} + A_{27} + A_{29})}{(A_{26} + A_{28} + A_{30})} + \frac{(A_{27} + A_{29} + A_{31})}{(A_{26} + A_{28} + A_{30})} \right) \quad [S1]$$

Average chain length (ACL) was calculated using a formula modified from ref. 17 as follows:

$$ACL = \frac{(25 \cdot A_{25}) + (27 \cdot A_{27}) + (29 \cdot A_{29}) + (31 \cdot A_{31})}{(A_{25} + A_{27} + A_{29} + A_{31})} \quad [S2]$$

In both Eqs. S1 and S2, *A* is the area under the chromatographic peak for each *n*-alkane of a specific chain length and for Eq. S2, 25, 27, 29, and 31 are the individual *n*-alkane chain lengths.

Additional Carbonate and Bulk Organic $\delta^{13}C$ Records. The $\delta^{13}C_{org}$ and $\delta^{13}C_{carb}$ patterns seen in the three marine sections shown in Fig. 2 of the main text are not limited to those localities. Here, we show seven other examples, all with consistent biological patterns at the extinction level (Fig. S2). These additional localities are Kuhjoch, Austria [the global stratotype section and point (GSSP) for the base Jurassic] (18, 19); Tiefengraben, Austria (20, 21); New York Canyon, Nevada (22); the Mingolsheim Core, Germany (23); and the Dorset Coast (24). We also provide new $\delta^{13}C_{org}$ data from the marine Blue Lias Formation at Lyme Regis, Dorset, England (collected by J.H.W.; see Table S1). The important feature to note is the initial excursion, similarity of the smaller positive excursion present at the higher resolution (St. Audrie's Bay, Kuhjoch, Tiefengraben, New York Canyon), and different degrees of a gradual positive excursion (Fig. S2) seen in the middle Hettangian in the long sections in both bulk organic and carbonate $\delta^{13}C$ (Lyme Regis, Mingolsheim, Dorset Coast, Kennebec Point, Val Adrara; refs. 23, 25) and seen in the Newark and Hartford data.

1. Eglinton G, Hamilton RJ (1967) Leaf epicuticular waxes. *Science* 156:1322–1335.
2. Spiker E, et al. (1988) Source of kerogen in black shales from the Hartford and Newark basins eastern United States. *US Geological Survey Bulletin* 1776:63–68.

3. Kotra RM, et al. (1988) Chemical composition and thermal maturity of kerogen and phytoclasts of the Newark Supergroup in the Hartford basin. *U.S. Geological Survey Bulletin* 1776:68–74.

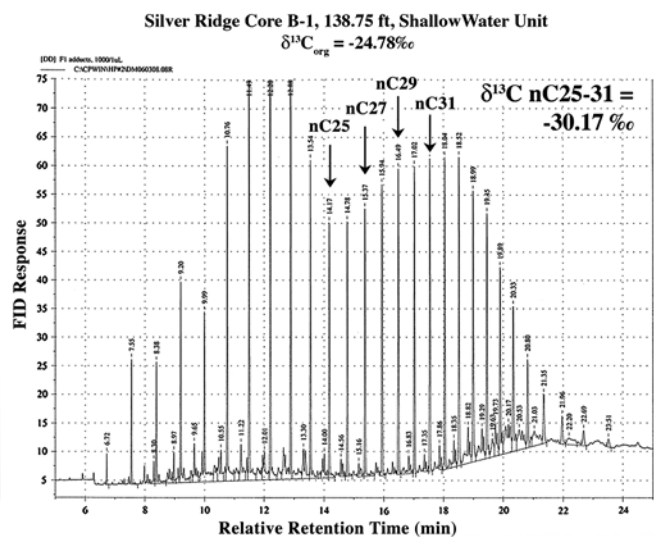
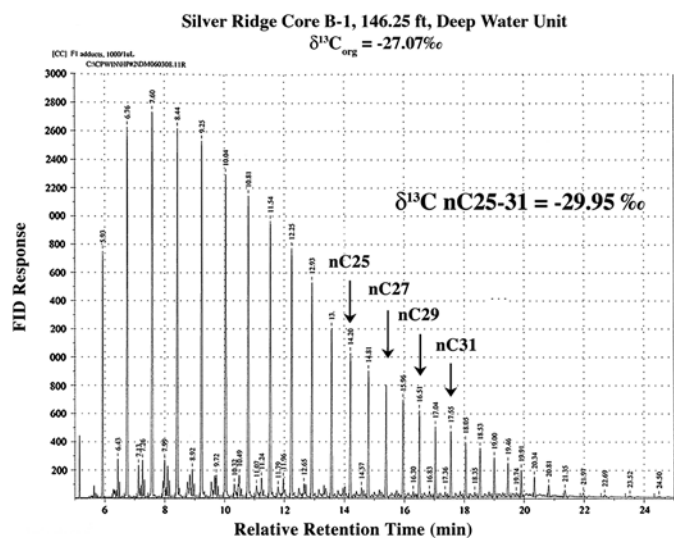
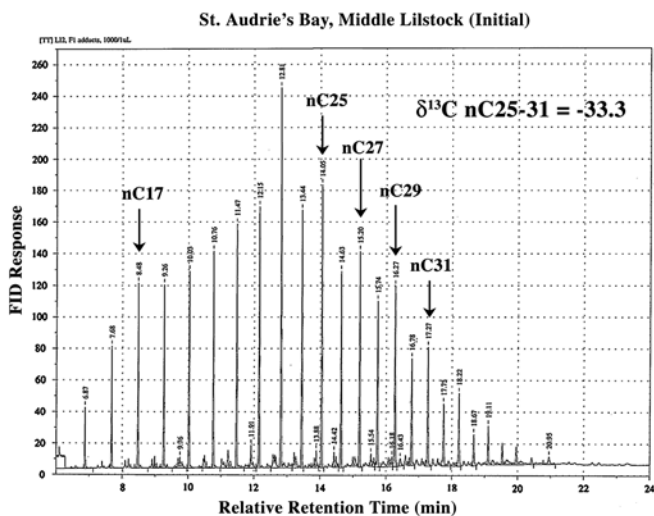
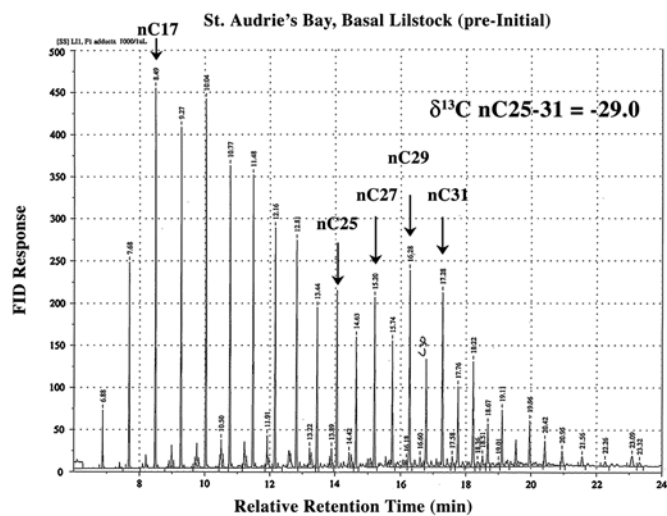


Fig. S1. Comparison between flame ion detector traces of samples from St. Audrie's Bay (above), and the Hartford basin (below) (from Dataset S1).

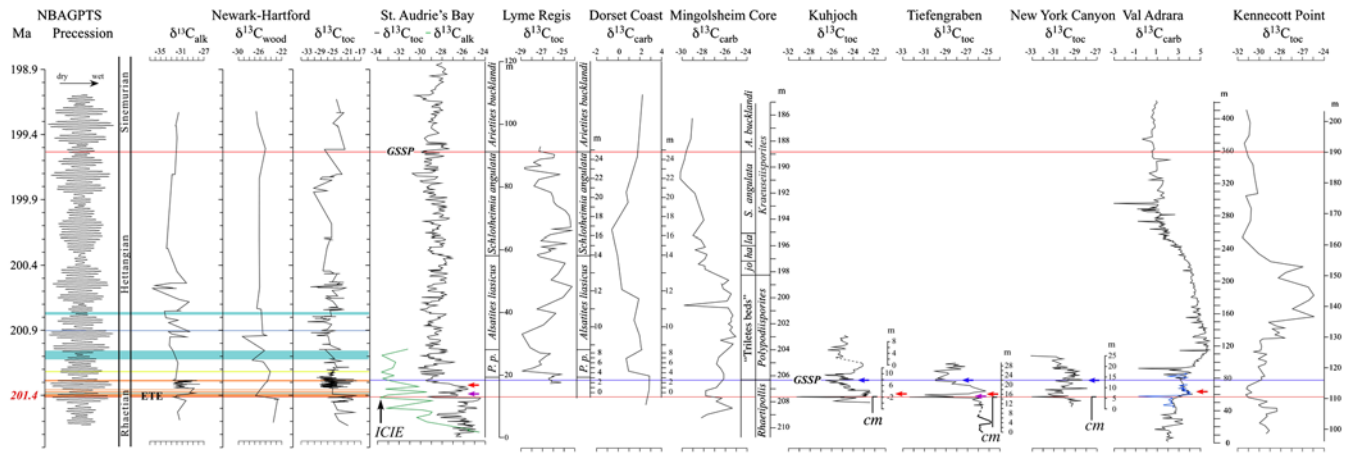


Fig. S2. Auxillary sections of $\delta^{13}C_{org}$ and $\delta^{13}C_{carb}$ from various localities compared to the Newark–Hartford, St. Audrie’s Bay, and Kennecott Point and Val Adrara data. These are: Lyme Regis, Dorset, England (see Table S1); the Dorset Coast (24); Mingolsheim Core, Germany (23); Kuhjoch, Austria (the GSSP for the base Jurassic) (18); Tiefengraben, Austria (20); New York Canyon, Nevada (22); and Val Adrara, Italy (23). Red lines are the Hettangian–Sinemurian boundary above and the main extinction level below. The blue curve in the Val Adrara data is from ref. 25 added by ref. 23 to their data. The $\delta^{13}C_{carb}$ samples for Val Adrara are bulk carbonate, but those for the Dorset Coast are nonscreened oysters (24). All the short sections and St. Audrie’s Bay were correlated following refs. 21 or 22. The other correlations are original. Black arrows point to the initial excursion; blue arrows indicate the position of the first appearance of the ammonite *Psiloceras spelae*, which has been picked as the taxon marking the base of the Jurassic at the newly identified GSSP (19) except at St. Audrie’s Bay where it represents the relative position of where it should occur based on ref. (21); red arrows mark the last appearance of *Rhaetipollis germanicus*; and purple arrows mark the last occurrence of conodonts. Abbreviations are BA, Blue Anchor Formation; buck Z, bucklandi Zone; cm, last occurrence of the Triassic ammonite *Choristoceras*; ha, *P. hagenowi*; jo, *C. johnstoni*; L, Lilstock Formation; la, *A. laqueus*; M, main isotopic excursion; pla Z, planorbis Zone; Westb, Westbury Formation. Other symbols, colors, and notation as in main text Fig. 4.

Table S1. $\delta^{13}C_{org}$ data from Lyme Regis

| Midpoints, m | $\delta^{13}C$ | Sample identification number | Midpoints, m | $\delta^{13}C$ | Sample identification number |
|--------------|----------------|------------------------------|--------------|----------------|------------------------------|
| 0 | | | 14.70 | -25.78 | 15.10.05.16 |
| 2.12 | -26.26 | 15.10.05.50 | 14.80 | -26.18 | 15.10.05.17 |
| 2.32 | -25.18 | 15.10.05.51 | 14.95 | -27.10 | 15.10.05.18 |
| 2.50 | -26.18 | 15.10.05.52 | 15.25 | -24.74 | 15.10.05.19 |
| 2.68 | -26.10 | 15.10.05.a1 | 15.55 | -27.19 | 15.10.05.20 |
| 2.85 | -26.32 | 15.10.05.a2 | 15.85 | -26.77 | 15.10.05.21 |
| 3.11 | -26.43 | 15.10.05.a3 ss | 16.15 | -26.26 | 15.10.05.50 |
| 3.36 | -26.10 | 15.10.05.A4 | 16.57 | -24.24 | 15.10.05.23 |
| 3.54 | -26.07 | 15.10.05.a5 | 16.73 | -26.02 | 15.10.05.24 |
| 3.82 | -25.19 | 17.10.05 | 16.92 | -24.29 | 15.10.05.24b |
| 4.45 | -28.94 | 17.10.05.p3 | 17.59 | -24.34 | 15.10.05.25 |
| 5.02 | -27.92 | 17.10.05.p4 | 18.19 | -24.45 | 15.10.05.26 |
| 5.63 | -27.12 | 17.10.05.pb2 | 18.64 | -24.83 | 15.10.05.27 |
| 6.21 | -27.33 | 15.10.05.01 | 19.20 | -25.64 | 15.10.05.28 |
| 7.20 | -26.63 | 17.10.05.pb 2B | 19.55 | -25.93 | 15.10.05.29 |
| 7.59 | -26.29 | 17.10.05.pb 2a | 20.01 | -25.99 | 15.10.05.30 |
| 7.75 | -27.27 | 17.10.05.pb | 20.56 | -26.18 | 15.10.05.31 |
| 9.49 | -28.97 | 15.10.05.02 | 21.22 | -27.82 | 15.10.05.31 |
| 10.03 | -26.92 | 15.10.05.03 | 21.87 | -27.35 | 15.10.05.32 |
| 10.69 | -25.73 | 15.10.05.04 | 22.41 | -25.37 | 15.10.05.33 |
| 10.92 | -27.53 | 15.10.05.5 | 22.85 | -28.07 | 15.10.05.34 |
| 11.59 | -25.02 | 15.10.05.06 | 23.01 | -28.74 | 16.10.05.0 |
| 12.25 | -24.16 | 15.10.05.07 | 23.14 | -28.72 | 15.10.05.34B |
| 12.61 | -26.17 | 15.10.05.08 | 23.34 | -27.17 | 15.10.05.35 |
| 12.95 | -25.52 | 15.10.05.09 | 23.66 | -27.85 | 16.10.05.01 |
| 13.59 | -24.83 | 15.10.05.10 | 24.01 | -27.21 | 15.10.05.36b |
| 13.95 | -27.38 | 15.10.05.11 | 24.16 | -25.92 | 15.10.05.37 |
| 14.13 | -27.51 | 15.10.05.12 | 24.46 | -25.84 | 15.10.05.47 |
| 14.33 | -26.72 | 15.10.05.13 | 24.81 | -27.32 | 16.10.05.04 |
| 14.50 | -26.17 | 15.10.05.14 | 25.08 | -27.31 | 16.10.05.05 |
| 14.63 | -26.45 | 15.10.05.15 | 25.33 | -27.22 | 16.10.05.07 |

Other Supporting Information Files

- [Dataset S1 \(XLS\)](#)
- [Dataset S2 \(XLS\)](#)
- [Dataset S3 \(XLS\)](#)